J Intell Robot Syst (2018) 91:181–192
https://doi.org/10.1007/s10846-017-0678-3

Design of a Bio-Inspired Autonomous Underwater Robot

Daniele Costa[1] · Giacomo Palmieri[1] · Matteo-Claudio Palpacelli[1] · Luca Panebianco[2] · David Scaradozzi[2,3]

Received: 18 January 2017 / Accepted: 30 June 2017 / Published online: 25 September 2017

Abstract The following paper presents the design and fabrication of an *ostraciiform* swimming robot and its navigation control and guidance system. Compared to other biomimetic vehicles, the chosen architecture has a lower propulsive efficiency but is easier to waterproof and capable to withstand greater pressures. To generate the alternating motion of the robot bio-inspired thruster, namely a plane fin, a transmission system was designed to replace the direct drive widely adopted in underwater biomimetic vehicles. The mechanical efficiency of two alternative mechanisms capable to actuate the fin were computed according to a preliminary sizing of the robot and its targeted swimming performances. Therefore, the more suitable solution was manufactured and installed aboard. At the same time, a proper navigation, guidance and control architecture (NGC) was designed and then integrated in the robot main controller. The proposed solution allows the vehicle to perform different missions autonomously once their profiles are received from the base station. Preliminary tests results and future works are discussed in the final conclusions.

Keywords Biomimetics · AUV · Swim mechanics · Robotic fish · NGC systems

✉ Daniele Costa
d.costa@pm.univpm.it

Giacomo Palmieri
g.palmieri@univpm.it

Matteo-Claudio Palpacelli
m.palpacelli@univpm.it

Luca Panebianco
l.panebianco@pm.univpm.it

David Scaradozzi
d.scaradozzi@staff.univpm.it

[1] Department of Industrial Engineering & Mathematical Sciences (DIISM), Polytechnic University of Marche, Ancona, Italy

[2] Department of Information Engineering (DII), Polytechnic University of Marche, Ancona, Italy

[3] Laboratoire des Sciences de l'Information et des Systèmes Equipe I&M (ESIL) – CNRS, Marseille, France

1 Introduction

In the field of Autonomous Underwater Vehicles, AUVs, biological inspirations are sought after and then adopted as part of the ongoing search for technological improvements, specifically in terms of maneuverability and thrust efficiency. Fish, in fact, are generally faster than traditional AUVs, both in terms of absolute velocity and relative velocity (normalized with respect to their body length, BL) [1]. Furthermore, biological systems turnabout maneuvers are characterized by a normalized radius of curvature R/BL lower than one, while AUVs belong to the range $2<R/BL<6$ [1]. Finally, the Cost of Transport (COT), which measures the energy spent to swim at a given speed, is significantly lower in marine animals with respect to AUVs [1].

The possibility to replicate successfully the various swimming modes that fish evolved in thousands of years depends from the understanding of the fluid mechanics principles applied to marine animals' locomotion as well as from the capacity to construct suitable actuation and control systems.

According to swim mechanics, a propulsive thrust originates by the momentum transfer due to the relative motion between the body of the fish and the surrounding water

[2]. In Body and Caudal Fin (BCF) locomotion, the body of the fish is bent by the passage of a propulsive wave that propagates backwards and faster with respect to the swimming velocity, up to the caudal fin. Breder's classification [3] further expands BCF locomotion in five swimming modes according to the percentage of the fish body that participates to thrust generation, Fig. 1. While *anguilliform*, *sub-carangiform*, *carangiform* and *thunniform* are *undulatory* modes, *ostraciiform* is a pure *oscillatory* swimming mode. The portion of the fish body bent by the passage of the propulsive wave shrinks going from *anguilliform* to *thunniform*, at the expense of maneuverability. On the contrary, efficiency is maximal when the propulsive wave is confined to the rigid caudal fin of *thunniform* swimmers [4]. Finally, in *ostraciiform* locomotion, thrust is generated by the pure oscillatory rotation of the caudal fin; this mode is associated to the lowest efficiency among BCF swimmers (50%), while the propulsive efficiency of small UVs is under 40% [5].

Several examples of bio-inspired AUVs can be mentioned and a complete review is given in [6]. The first biomimetic robotic fish were the MIT RoboTuna [7] and Hirata's RoboPike [8], manufactured in 1995. Both these robots used a serial N-joint mechanism to bend their tail and generate thrust. A few years later, Draper Institute created the fully autonomous Vorticity Control Unmanned Undersea Vehicle (VCUUV) [9] that employs hydraulic actuators to drive the multi-link mechanism in its tail. In the early 2000s, Fukuda et al. developed a new series of biomimetic underwater micro robots using Ionic Polymer-Metal Composites (IPMC) as tail actuators [10]. In 2008, Victoria University tested a biomimetic robot propelled by a continuously flexible tail bent by Shape Memory Alloys (SMA) [11]. At the same time, Kodati et al. manufactured the *ostraciiform* robotic fish MARCO [12]. One year later, Alvarado et al. tested the swimming performances of compliant fish-like robots [13]. A similar design was used by Stefanini et al. [14] and Kruusmaa et al. [15] a few years later.

The aim of the present work is to design a bio-inspired underwater vehicle exploiting the principles of fish swim mechanics as well as to integrate a suitable navigation, guidance and control system that allows the robot to perform tasks autonomously. On the basis of the aforementioned studies, main drivers of the project are:

i To design an underwater vehicle inspired to the swim mechanics of *ostraciiform* swimmers. As stated before, *ostraciiform* locomotion is not the most efficient mode but the mechanical system that realize such kind of propulsion, consisting in an oscillating caudal fin, is simple, cheap and easy to replicate. Furthermore, it may represent a basic module that can be used to design more complex bio-inspired propulsion systems such as multi-segmented tails.

ii To generate the alternating motion of the fin by means of a transmission system that converts the continuous rotation of the drive in a harmonic oscillation; in this way, the effort required to the control system is reduced, being sufficient a constant velocity setting for the motor. On the other hand, a direct drive connected to the tail would require position control in order to realize a sinusoidal motion.

iii To design a control system that allows the robot to perform different missions autonomously and to manage various types of payloads (sensors, communication device, actuators and so on). Since these requirements demand a high degree of modularity and abstraction, the multi-agent architecture was chosen to design the system.

After a brief recall on the alternative architectures employed to design a robotic fish, Section 2 introduces the preliminary design of the robot based on its mission targets. Section 3 is dedicated to the actuation systems designed to drive the caudal fin; the authors devised two different transmission mechanisms and an analysis of their respective features and is presented is this paper. The NGC system developed and integrated in the robot is described in Section 4, while its mechatronic design and the experimental tests are shown in Section 5. Finally, Section 6 discusses the conclusions and presents future works.

2 Preliminary Sizing

As stated in the previous section, thrust generation in BCF locomotion is due to the passage of a propulsive wave along the posterior, flexible part of the fish body. According to Lighthill's *elongated body theory* [16], the lateral displacements exhibited by the bodies of slender fish can be approximated by the following formula:

$$y_{body}(x,t) = \left(c_1 x + c_2 x^2\right) \sin(kx + \omega t) \tag{1}$$

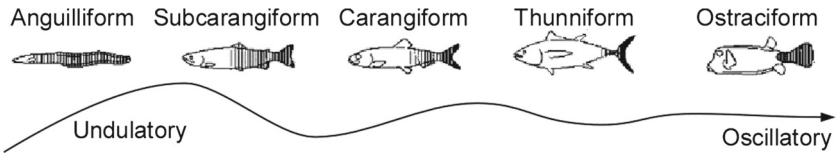

Fig. 1 BCF oscillatory and undulatory swimming modes [3]

where $k = 2\pi/\lambda$ is the wave number and $\omega = 2\pi f$ is the undulating pulse. Given the slenderness hypothesis, the former expression best suits to *anguilliform* and *sub-carangiform* locomotion. A modified theory was also provided by Lighthill to account for large lateral body motion in *carangiform* and *thunniform* swimming [17].

In order to comply with the aforementioned theory, three alternative ways to design a robotic fish have been identified and exploited in the last two decades, as showed in Fig. 2 [18].

The "oscillating plate" design (Fig. 2a) consists of a rigid hull and an oscillating plate connected to the body through a revolute joint. Just like an *ostraciiform* swimmers, it has a low propulsive efficiency; however, this architecture is simple, inexpensive and its perfectly rigid body makes it is much simpler to waterproof and capable of withstanding greater depths. The robot shown in [12] is an example of this style.

The "traveling wave" design method (Fig. 2b) aims to produce a smooth and continuously flexible hull. Thrust is produced by the undulatory motions traveling through the whole body with an amplitude that increases backwards as stated by expression (1). This style allows the design of extremely small robots [10] and compliant robots such as those in [13–15].

The "flapping wing" design (Fig. 2c) consists of an anterior rigid head and a piecewise flexible tail driven by an N-joint serial mechanism. Expression (2) is then respected in a finite number of points only and different methods exist to optimize the relative length of the links [19, 20]. The robots in [7–9] are examples of this style.

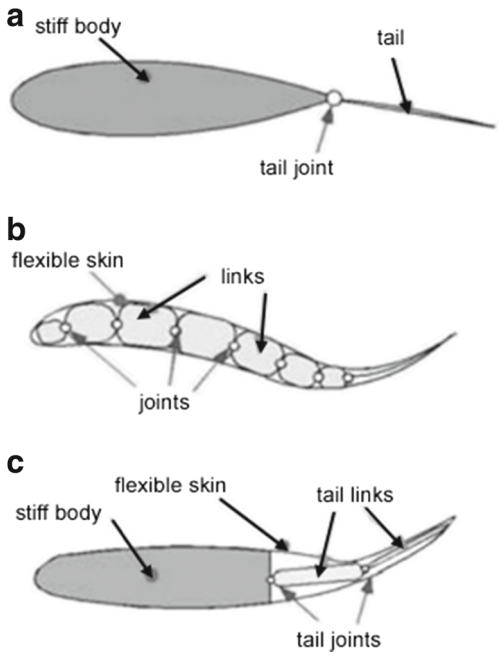

Fig. 2 Robotic fish alternative design [18]: **a** oscillating plate, **b** traveling wave, **c** wing

At this stage of development, the authors aim to design an autonomous underwater vehicle capable to perform well-defined missions for marine exploration, while exploiting the principles of fish swim mechanics: particularly, it has to navigate to a list of point of interest at 20–40 meters depth and perform some actions. Then, among the aforementioned architectures, the oscillating plate style was chosen due to its simplicity to build and easiness to waterproof. Due to this choice and according to [21], a 0.5 BL/s cruising speed is a reasonable targeted velocity for an *ostraciiform* swimming robot.

The vehicle main components are the cylindrical rigid fore body and the tail section, where the caudal fin is connected to the robot stern through a revolute joint. In a previous work, the authors showed the existence of a linear relationship between the cylinder radius and the caudal fin average height, opening the possibility for a parametric sizing of the vehicle [22]:

$$R = \lambda H_{av} \;\; \lambda = f\,(St,\, \theta_0,\, \eta_h) \tag{2}$$

where R is the fore body radius, H_{av} is the average height of the fin and λ is a function of the *Strouhal* number, the oscillating amplitude θ_0 and the *ostraciiform* swimming efficiency η_h. For a BCF swimmer, the *Strouhal* number is a dimensionless parameter defined as follows:

$$\begin{aligned} St &= \tfrac{f\,A}{U} \\ A &= 2B\sin\theta_0 \end{aligned} \tag{3}$$

where U is the average swimming speed, f is the caudal fin flapping frequency and A is the wake width, normally approximated as the amplitude of a fin stroke by means of

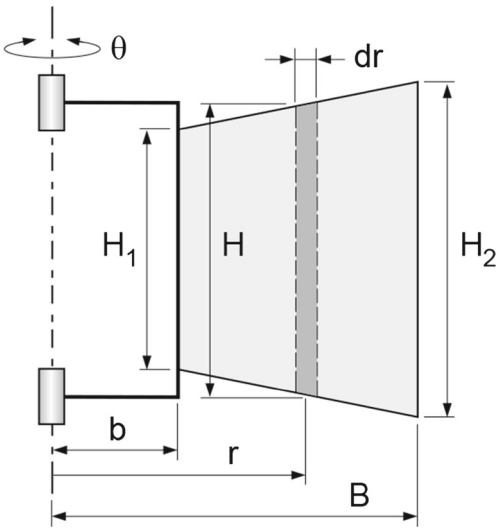

Fig. 3 Geometry of the caudal fin

Table 1 Caudal fin geometry and inertia

Material: 6060 Aluminum alloy				
H_1 [mm]	H_2 [mm]	B [mm]	b [mm]	m [kg]
150	210	215	70	0.166

its total length B [12], Fig. 3. Thrust generation in oscillating foils is optimal when the *Strouhal* number falls inside the $0.25 \div 0.35$ interval [23]. Therefore, once a project value for St is chosen inside the prescribed interval, while θ_0 and η_h are opportunely set, the caudal fin geometry and flapping frequency are consequently determined as a function of the cylinder radius and the targeted cruising speed. The procedure followed by the authors to obtain expression (2) is detailed in the final Appendix.

The body radius lower bound is set by the payload housed in the fore section. The largest components are the robot battery pack and its main controller, namely a National Instrument myRIO board. Since the transversal section of this device is a 90 mm $\times$ 25 mm rectangle, the fore body radius was set to 60 mm. Therefore, according to expression (2), where the amplitude of the oscillation θ_0 is chosen equal to 15° to prevent flow separation [18], the caudal fin average height is equal to 170 mm. Table 1 summarizes the fin geometry and inertia. Regarding its kinematics, a 1.67 Hz oscillation frequency results from expression (3).

3 Actuation Design

As discussed in [21, 22], the optimal motion law for the fin of an *ostraciiform* swimmer is of the type:

$$\theta = \theta_0 \cos(2\pi f t) \tag{4}$$

The most common solution adopted to generate a motion law similar to the former expression is by way of a rotary electric servomotor that provides alternating displacements. Therefore, position control is required to comply with expression (4).

Two different solution was designed by the authors to replace the rotary actuator with a transmission system that converts the continuous rotation of the drive into a harmonic oscillation. The first mechanical system able to generate a motion law much similar to expression (4) is the Scotch-Yoke mechanism shown in Fig. 4. The input rotation angle $\varphi = \omega t$ of the motor is transformed into harmonic oscillation $\theta(t)$ of the output member, which is fixed with the caudal fin. The output angle θ and the motor rotation φ are related by the expression:

$$\tan\theta = \frac{h}{L}\cos\varphi \tag{5}$$

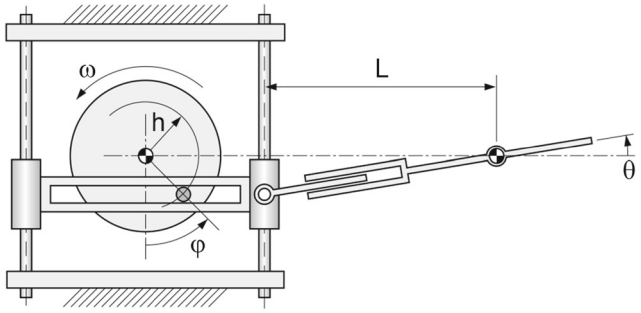

Fig. 4 Scotch-Yoke mechanism

where h and L are the geometric parameters outlined in the kinematic scheme of Fig. 5. Expression (5) leads to the following velocity law:

$$\dot{\theta} = -\left(\frac{hL\sin\varphi}{L^2 + h^2\cos^2\varphi}\right)\omega \quad (\omega = \dot{\varphi}) \tag{6}$$

Expression (5) slightly differs from Eq. 4, being the angle θ the argument of a tangent function; nevertheless, it results easy to demonstrate that Eq. 5, as well as Eq. 6, can be approximated to a pure sinusoidal function if $h/L = \tan\theta_0 \ll 1$. Since for θ_0 equal to 15° it results $h/L \simeq 0.27$, the approximation is reasonable and the following simplified kinematic laws can be considered:

$$\begin{aligned} &\theta = \tfrac{h}{L}\cos\varphi \quad \dot{\theta} = -\left(\frac{h}{L}\sin\varphi\right)\omega \\ &\ddot{\theta} = -\left[\left(\frac{h}{L}\sin\varphi\right)\dot{\omega} + \left(\frac{h}{L}\cos\varphi\right)\omega^2\right] \end{aligned} \tag{7}$$

The second mechanism, which exactly replies the fin motion obtained with the Scotch-Yoke mechanism, is based on a spatial cam kinematic joint. This device is known in literature [24] but, to the best of the authors' knowledge, it was never adopted to actuate the tail of an underwater biomimetic robot. In such a mechanism, as shown in the

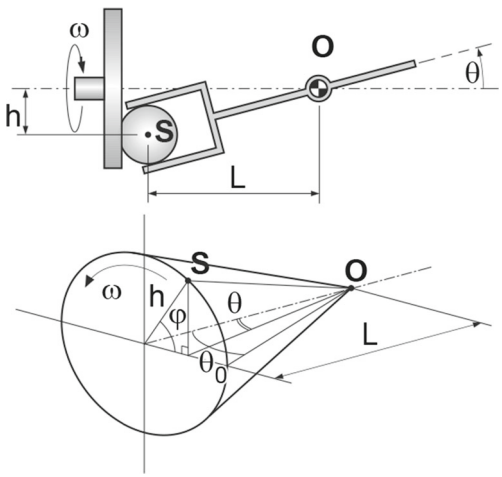

Fig. 5 Cam-like mechanism kinematic scheme

CAD model of Fig. 5, a driving disk A has a drive-sphere B that engages in a rectangular groove in a driven member C. The output shaft is rigidly connected with driven member C and is capable to pivot freely in a support block D. With the new meaning of the geometrical parameters h and L, defined in the kinematic scheme of Fig. 5, Eqs. 5 and 6 still holds; therefore, at the same condition for the ratio h/L, approximated motion laws (7) are still acceptable for the present kinematic solution. By means of these solutions, the position control required to comply with expression (4) is replaced with a constant velocity setting imposed on the drive, at least during cruising speed navigation.

It is here presented a simple analytic hydrodynamic model used to estimate the torque acting on the motor shaft due to the fin oscillation at a certain frequency. The total torque T due to the external loads, computed with respect to the fin shaft, is composed by three terms:

$$T_{total} = T_{damp} + T_{fin} + T_{am} \tag{8}$$

The term T_{am} is due to the acceleration of the added mass of water surrounding the fin, T_{damp} is the effect of the drag force that is opposed to the fin motion, while T_{fin} represents the torque component given by the inertia of the fin. This various terms in the former equation are computed according to the expressions provided in the final Appendix of the present paper.

Equation 8 can be recomputed with respect to the driving shaft angular velocity and acceleration by means of Eq. 7 and by applying the work-kinetic energy theorem:

$$T_{total}\dot{\theta} = T_{total}\left(\frac{h}{L}\sin\varphi\right)\omega = T_{motor}\omega \tag{9}$$

Equation 9 demonstrates that the application of a transmission system like those proposed in this paper, introduces a gear ratio proportional to h/L which in turns is equal to the tangent of the fin oscillation amplitude θ_0. Therefore, as stated before, it results $h/L \simeq 0.27$and the same factor is applied to the torque sensed by the motor, which allows the selection of a smaller drive.

The former conclusion applies to both the Scotch-Yoke and the cam-like mechanism. Figure 6 shows the torques sensed by the motor when friction forces are applied to the joints. Table 2 summarizes the dynamic friction coefficients introduced in the analytic models of the transmission mechanisms.

Compared to the frictionless transmission system, the mechanical efficiency of the cam-like mechanism is 79.2%, while the corresponding value for the Scotch-Yoke solution is lower, namely 70.6%, due to friction losses in the prismatic joints and in the coupling box. In the same way, the maximum torques sensed by the drive when the proposed solutions are applied to the fin shaft, are respectively 9% higher for the cam-like mechanism and 17% higher for the Scotch-Yoke.

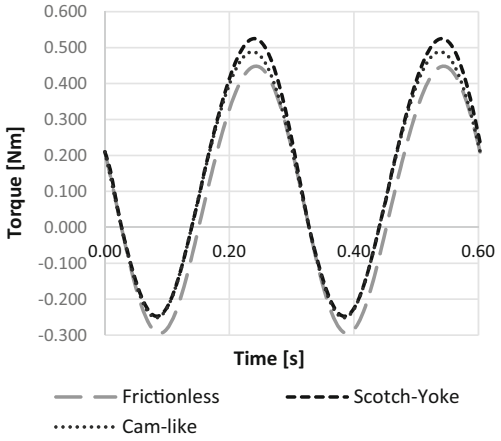

Fig. 6 Total torque sensed by the motor

A further comparison is carried on by analyzing the proposed solution from a manufacturing point of view. Figure 7 shows a virtual prototype of both mechanisms: compared to the cam-like transmission, the Scotch-Yoke solution is:

i Less compact: in fact, it results 25 mm longer in the longitudinal direction (i.e. the robot roll axis), which in turns, considering the tail cross section, corresponds to a +4% of the vehicle total mass in water (calculated according to a preliminary assessment of the vehicle volume required to house the onboard payload).
ii More expensive: due to a larger number of parts and components. Furthermore, the cost to purchase commercial prismatic joints grows quickly when their size falls under 8–10 mm.
iii Harder to manufacture: in order to prevent the risk of vibrations in the prismatic joints, their rails must be carefully aligned.

According to the previous considerations, the cam-like mechanism was used as the fin transmission system while a 12 V DC brushed motor with a 70:1 gearbox was chosen as its drive. This gear ratio allows the motor to operate near the highest efficiency condition (https://www.pololu.com/product/2825).

Table 2 Caudal fin geometry and inertia

Scotch-Yoke mechanism	
Pin (steel) – Slot (PTFE)	0.09
Prismatic Joints	0.25
Coupling box	0.18
Cam-like mechanism	
Sphere (steel) – Groove (PTFE)	0.09

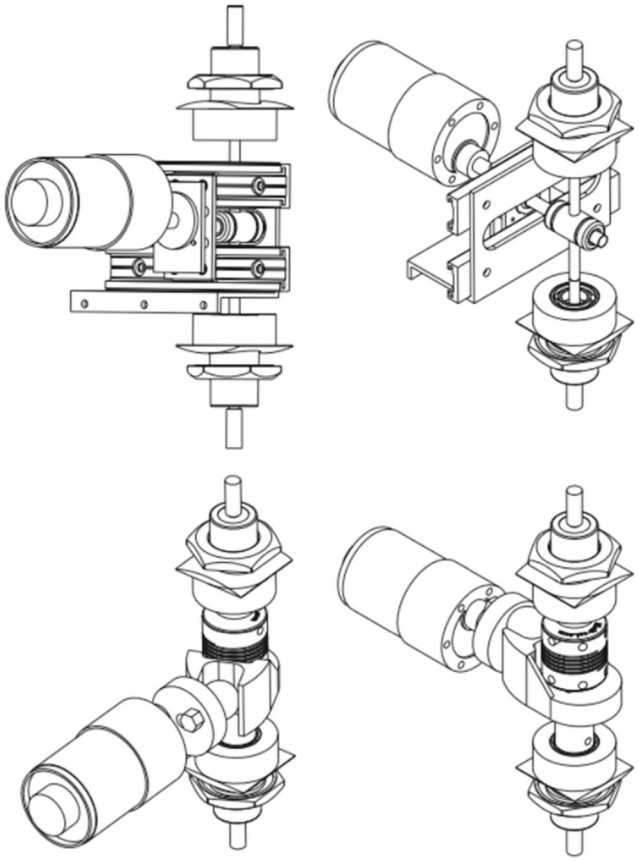

Fig. 7 Scotch-Yoke mechanism (upper drawings) and cam-like mechanism (lower drawings) CAD assemblies

4 Navigation Guidance and Control System

The low level fin system, already described in the previous Sections, is governed by the fish NGC structure in order to allow the robot to perform different missions autonomously. Furthermore, the global NGC system has to manage various types of payloads (communication devices, sensors, actuators). Since these requirements demand a high degree of modularity and abstraction, the multi-agent architecture was chosen. Because of a lack of access to satellite systems while the robot is under water and the requirement to have a low-cost and stand-alone platform that does not rely on precise but costly solutions like the acoustic localization devices largely employed in the underwater environment, the navigation system is a critical aspect of the work proposed by the authors.

The type of mission that this vehicle has to perform at this stage of the development is the execution of a well-defined mission for marine exploration, expressed by means of a list of point of interest to navigate to and actions to perform. Therefore, the vehicle does not need complex planning capabilities.

AUVs typically proceed by dead reckoning for long intervals, relying only on the information provided by on-board sensors. Allotta et al. [25, 26] proposed an underwater navigation system, developed inside the ARROWS project, that exploits the measurements from various sensors and relies on an unscented Kalman filter (UKF) or an extended Kalman filter (EKF) for the state estimation. The measured quantities are processed while the vehicle navigates in dead reckoning to approximate its dynamics. These results are then used to compute the motor control signals: the thrusts produced by the motors allow the vehicle to follow the desired dynamics while the sensor suite provides the real physical outputs to be used in the UKF-based or EKF-based navigation system.

In order to perform different type of missions for different activities related to underwater research, the designed vehicle must be able to manage different type of payload, such as sensors, underwater communication devices, actuators or manipulators. In order to satisfy the former requirements, the robot mechatronic architecture was designed as a system characterized by a high degree of modularity and abstraction, Fig. 8.

The intelligent control architecture of the bio-inspired underwater robot described in this paper can be summarized by its two main components: the Low Level and the High Level, while the union of these two is the NGC system.

The NGC system communicates with the base station, which has two main purposes: to create, modify and upload a mission (the mission creator) and to remotely control the AUV through a custom-made interface (the Remote User Interface). The custom-made interface is used to perform tests, initiate the mission and gather data.

The Low Level is made up by an array of devices connected with the High Level through the industrial I^2C bus. There are two types of devices: commercial off-the-shelf (COTS) devices, such as the Inertial Measurement Unit (IMU) the Global Positioning System (GPS) and the depth meter, and custom-made, such as the energy and thruster manager. The custom-made devices have a minimum degree of autonomy in case of emergency, which involves taking the system into a safe steady state with a faster and predictable response to malfunctions (such as low battery or water leaks inside the vehicle). This approach avoids single point failures in the NGC system if there is a major fail related to the High Level.

When a new device is attached to the shared bus, a module of the High Level component is able to discover it and communicate with it in a transparent way.

The High-Level component of the NGC system is based on well-established techniques frequently adopted and tested in AUVs as well as in remotely operated vehicles navigation [27–30]. In addition, this component implemented on a Linux Real-Time device (NI-MyRIO) follows the Multi

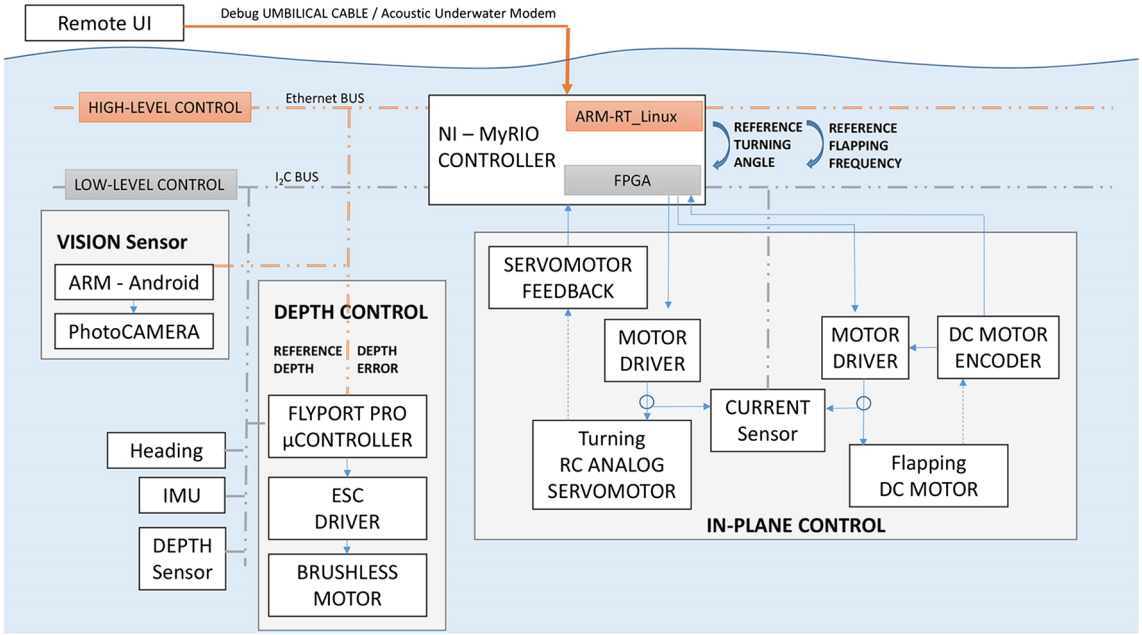

Fig. 8 NGC hardware architecture of the robot

Agents System characterization theory (MAS) used by the authors to model a home automation system [31]. This type of approach allows to increase the system abstraction and modularity, in order to design distributed entities (agents) able to fulfill different tasks autonomously. The agents (made as LabVIEW *.VI files) can read data and interact with the Low Level devices through a Blackboard-type software module that maintains synchronized all the data of the NGC system. In the present work, these techniques are simplified in order to make the vehicle components purely reactive following the intelligent agent definition provided by Wooldridge in [32]. The developed agents, in fact, lack on proactiveness and social capabilities. Cognitive capabilities are not required either for the type of missions performed by the present vehicle but the control architecture is ready to consider it as to connect with ROS compatible robot agencies.

Simplification is also needed because of the on-board hardware limitations. The software architecture comprises five threads (one for each agent): navigation, guide, low level, communication manager and log manager. Each thread manages a specific section of the entire vehicle autonomy. The modules are synchronized with each other in order to allow for the exchange of messages and information, Fig. 9.

The navigation thread manages the different functioning modalities: manual, automatic and emergency. The system starts in manual mode, where the user can manually control and monitor the status of the robot like a ROV. If

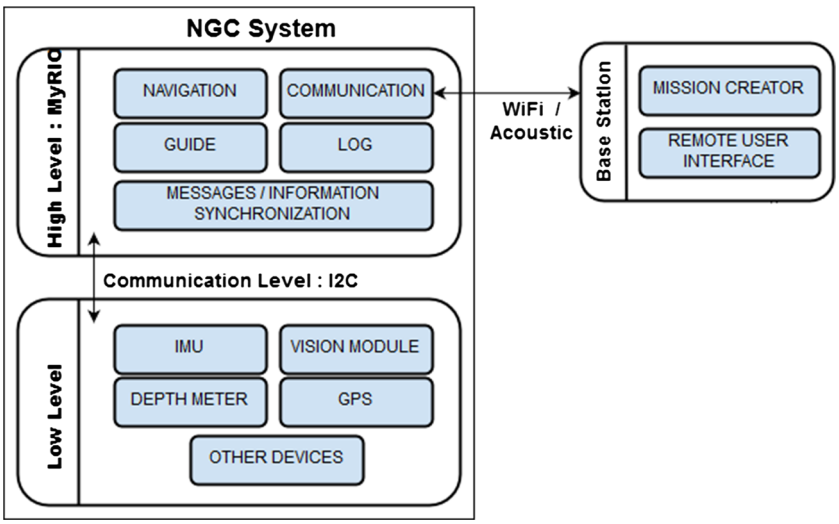

Fig. 9 Multi-agents architecture of the robot

necessary, it is also possible to enable or disable the auto-depth and auto-heading algorithms. The system changes from manual mode to automatic mode when the start command is received. Once the automatic mode is active, the mission executor processes the loaded mission. The latter is described by many tasks and a mission timeout. When the mission timeout is reached, the mission is over. Each task has its own timeout and is arranged as a finite state machine. A state is composed of a series of elements that allow the system to perform cyclically repeatable actions, as well as actions conditioned by the system status and its global variables, like depth and heading, along with battery and thrusters operative status. For example, one element of the state structure represents a single vehicle moving action to be sent to the guide module. Before processing the following element, the mission executor waits for the end signal from the guide module. The mission is editable and loadable to the vehicle through a proper graphical user interface (GUI) and it is exchanged and stored as a JavaScript Object Notation (JSON) string. When all the states of a task have been executed or the task timeout is reached, the mission executor processes the following task. When the mission reaches a timeout or all the tasks have been handled, the automatic mode manages the surfacing action of the vehicle. Once the vehicle is out of water, the system switches to manual mode. If a critical condition is experienced, such as low battery or a hardware failure, the mission terminates. When the external emergency switch is triggered, the entire system enters in emergency mode and any thruster is shut down until the external switch is triggered again.

This module is executed with a period of 100 ms. The reading and writing time, along with the transmission of a message between different threads in the system are not deterministic but they were estimated to be on the order of 10 ms during tests.

The guide module performs the commands sent from the navigation module while sending a feedback. The guide module also manages the auto-depth and auto-heading algorithms. The module execution period is 100 ms.

The low level module communicates with the systems connected with the low level bus (I^2C) and keeps the system status information up-to-date. In addition, the low level module updates the status of all the connected devices that the guide module has access to. This module is executed every 10ms. Each device attached to the bus has a proper read/write period that is a multiple of that of the module, and is arranged to avoid overlapping with other requests generated within a single module execution. The code is developed with non-blocking criteria.

The communication manager communicates with the base station primarily. Specifically, it transforms the information received and transmitted through Wi-Fi or acoustic modem and the real time telemetry data in a file format that can be handled by the other software threads.

The final thread implements the log manager. It writes the log files in different formats and saves them in a USB pen-drive. These two modules are executed with a period of 100ms.

5 Vehicle Mechatronic Design and Testing

Economic constraints play a significant role in choosing the size of a vehicle. Minimizing dimensions generally reduce costs, but a lower bound exists due to the availability of the necessary production equipment. Furthermore, electronic and mechanical components become usually more expensive as their dimensions shrink. Therefore, a compromise choice has to be taken. In the present paper, the fore body cross-section radius was chosen according to the housed payload, as stated in Section 2. As a whole, the robot architecture consists of a two-module assembly: the body and the tail.

The body is composed by an aluminum cylindrical pressure hull, enclosed between two acetal neck flanges; a Perspex dome closes the forward-most flange. In order to prevent any water leakage, a double O-ring seal was created between the flange and the dome. This module is 400 mm long and the cylinder wall is 5 mm thick. The body houses a vertical thruster ducted inside a low-drag shaped sail manufactured by 3D-FDM technique. The propeller axis of rotation passes through the center of buoyancy of the entire vehicle in order to minimize the pitching moment during depth changing maneuvers. In order to allow the robot to steer and control its trajectory, two commercial horizontal thrusters were fixed on the sides of the vehicle, aligned with its roll axis. The aim of these components is to create a pure yawing moment during forward navigation, to adjust the robot heading. In future works, they will be replaced by pectoral fins.

The body also houses the onboard electronics that consists of a battery pack sized to complete a two-hour mission, the robot main controller (the NI myRIO), the IMU and three Photon micro-controllers used to manage the fin motor, the vertical and the horizontal thrusters. The Photon board is based on the wireless connectivity for embedded devices (WICED) architecture provided by Broadcom and combines a STM32 ARM Cortex M3 microcontroller and a Broadcom Wi-Fi chip.

The tail section consists of cylindrical cap obtained from a POM/acetal block. The forward-most part of this module is connected to the body by twelve bolted screws and a double O-ring seal prevents water leakages between the joining surfaces. A second Perspex dome closes the tail section while allows inspections of the fin actuation system. Finally, the tail hollow part houses the fin shaft, the cam-like mechanism and its drive.

As a whole, the vehicle is 600 mm long (or 800 mm including the fin) and has a mass of approximately 6 kg. The robot assembly was validated to safely reach 100 m without water leakages or structural damages, Fig. 10.

Pertaining to the targeted swimming performances stated in Section 2, the authors conducted various tests, in and out of the water, in order to calibrate the ACS712 current sensor they used to measure the current absorbed by the DC motor and thus estimate the total torque acting on it. These values will be also used to verify the analytic fluid dynamic models found in literature. The following experimental set-up was then arranged: the vehicle was immersed into a 2 m depth pool and a 100 rpm constant angular velocity was imposed to the drive by means of a PID controller, corresponding to the prescribed 1.67 Hz fin oscillation frequency. The inertial measurement unit recorded a 0.42 BL/s average forward speed, while the targeted swimming velocity, predicted by the model in [18], was 0.5 BL/s. A possible explanation was found by analyzing the motor current absorption and its angular velocity: when it spins at 100 rpm, the continuous torque provided is 0.47 Nm, which is higher than the maximum torque sensed by the motor when dynamic friction is not applied to the joints, as shown in Fig. 6. However, the maximum torque required to the drive, when friction is computed into the model, rises close to 0.5 Nm, which is higher than the maximum available torque at 100 rpm. This evidence is supported by the angular velocity read by the encoder: the motor actually slows down near the angular positions corresponding to the maximum values of the torque inside a cycle. Therefore, since propulsive thrust depends on the square of the drive angular speed, it is reasonable to expect a decrease in the robot average swimming velocity. However, since the aforementioned drop is limited to a small portion of the oscillation cycle, namely $\pm 5°$ around the angular positions corresponding to the maximum torque, and the dynamic model adopted by the authors only predicts the average forward speed according to the average propulsive power, it is tough to formulate a quantitatively relationship between the drive angular velocity drop and the swimming performances. This result can be achieved by measuring the propulsive thrust generated by the fin, which is left to future works.

A further explanation could lie in an overestimated *ostraciiform* swimming efficiency value, which depends from both the fish body shape and the fin [12]. Since the vehicle tail external shape is not optimized like the body of a boxfish, it is reasonable to assume that the incoming flow is disturbed by the shape corners of the hull joining elements (flanges, screws) with a resulting reduction of the propulsive efficiency.

Fig. 10 Robot prototype

6 Conclusions

AUVs propulsive efficiency and maneuverability can be improved by studying fish swimming modes and locomotion. Results analyzed on bibliography show that AUVs are still far from reproducing the performances of biological swimmers.

In the present work, a transmission mechanism was designed by the authors to actuate the caudal fin of an *ostraciiform* swimming vehicle. The proposed solution reduces the effort required to the motor control system because a constant angular velocity set, imposed to the drive, replaces the non-linear position control of a direct drive system such as a servomotor directly connected to the fin shaft. The cam-like mechanism represents an inexpensive solution, easy to manufacture, replicate and miniaturize. Therefore, it can be used to actuate a simple biomimetic robot or as a basic module applied to more complex bio-inspired propulsion systems.

The aforementioned transmission mechanism was designed according to a preliminary sizing of the vehicle once the mission objectives and the targeted swimming performances, namely the forward navigation velocity, were opportunely set. The experimental tests conducted on the robot showed a good correspondence between the predicted values and the actual results. However, more work is still to be done to correct the fluid-dynamic and multi-body models adopted by the authors.

Finally, a suitable NGC system based on the multi agents system theory has been developed and integrated in the robot main controller. The proposed system was successfully tested to manage the onboard electronics and the mechanical devices during forward navigation missions. In future works, the NGC system will be tested in a real case scenario.

Appendix

A biomimetic robot swimming in a straight path at average constant speed must generate enough thrust to balance the hydrodynamic drag exerted by the fluid:

$$D = \frac{1}{2}\rho_{water} c_D A_f U^2 \tag{10}$$

where ρ_{water} is the density of water, U is the targeted swimming speed and A_f is the wetted frontal surface of the vehicle. Appropriate values for the coefficient of drag c_D are function of the *Reynolds* number and are detailed in [33]. Therefore, in terms of power:

$$P_D = \frac{1}{2}\rho_{water} c_D A_f U^3 \tag{11}$$

According to the model provided by Tryantafyllou et al. in [18], a propulsive thrust is generated when an oscillating foil accelerates the equivalent added mass of water surrounding it. Therefore, calling $H(r)$ the height of the fin at distance r from its oscillation axis, Fig. 3, potential theory allows to express the water added mass per unit length $Q(r)$ as [34]:

$$Q(r) = \rho_{water}\pi H^2(r)/4 \tag{12}$$

As discussed before, the expression for the fin law of motion is:

$$\begin{aligned} \theta &= \theta_0 \cos(2\pi f t) \\ \dot{\theta} &= -2\pi \frac{StU}{2B\sin\theta_0}\theta_0 \sin(2\pi f t) \\ \ddot{\theta} &= -4\pi^2 \left(\frac{StU}{2B\sin\theta_0}\right)^2 \theta_0 \cos(2\pi f t) \end{aligned} \tag{13}$$

where the flapping frequency f was expressed in terms of the *Strouhal* number St, the swimming speed U and the fin length. Based on the scheme of Fig. 3, the total torque T_{am} due to the elementary added mass forces dF_{am} is thus computed, with respect to the fin oscillation axis, by the following expressions:

$$dF_{am} = \ddot{\theta} r Q(r) dr = r\ddot{\theta}\frac{\rho_{water}\pi H^2(r)}{4}dr \tag{14}$$

$$T_{am} = \int_{fin} r\, dF_{am} = \rho_{water}\pi\frac{H_{av}^2}{4}B^3\ddot{\theta} \tag{15}$$

The expression of the average swimming power P_{prop} during a period is finally obtained by multiplying the *ostraciiform* swimming propulsive efficiency η_h and the mean power required to accelerate the added mass of water surrounding the fin. This expression is equalled to the hydrodynamic drag power (11):

$$P_{prop} = \eta_h \overline{\left(\left|T_{am}\dot{\theta}\right|\right)} = P_D \tag{16}$$

The substitution of expressions (13) in Eq. 16 leads to the following sizing constraint:

$$R_{eq} = \lambda H_{av} \;\; \lambda = f(St,\, \theta_0,\, \eta_h) \tag{17}$$

where R_{eq} is the frontal surface equivalent radius, H_{av} is the average height of the fin and λ is a function of the *Strouhal* number, the oscillating amplitude θ_0 and the *ostraciiform* swimming efficiency η_h, primarily set to 50% [2, 18, 22].

According to the model in [22], the first two terms of Eq. 8 can be calculated as:

$$T_{damp} = \frac{\rho_{water} c_{damp}}{2}\left(\int_b^B Hr^3 dr\right)\dot{\theta}\left|\dot{\theta}\right| \tag{18}$$

$$T_{fin} = \left(\int_{-s/2}^{s/2}\int_b^B \rho_{fin}\left(r^2+s^2\right)Hdrds\right)\ddot{\theta} \tag{19}$$

where c_{damp} is the plate drag coefficient, ρ_{fin} is the density of fin and s represents the fin thickness.

References

1. Murphy, A.J., Haroutunian, M.: Using bio-inspiration to improve capabilities of underwater vehicles. In: 17th International Symposium on Unmanned Untethered Submersible Technology (UUST 2011), Portsmouth, pp. 20–31 (2011)
2. Sfakiotakis, M., Lane, D.M., Davies, J.B.C.: Review of fish swimming modes for aquatic locomotion. IEEE J. Ocean. Eng. **24**(2), 237–252 (1999)
3. Breder, C.M.: The locomotion of fish. Zoologica **4**, 159–256 (1926)
4. Anderson, J.M., Streitlien, K., Barrett, D.S., Triantafyllou, M.S.: Oscillating foils of high propulsive efficiency. J. Fluid Mech. **360**, 41–72 (1998)
5. Wang, Z., Hang, G., Li, J., Wang, Y., Xiao, K.: A micro robot fish with embedded SMA wire actuated flexible biomimetic fish. Sensors Actuators A Phys. Elsevier **144**(2), 354–360 (2008)
6. Scaradozzi, D., Palmieri, G., Costa, D., Pinelli, A.: BCF swimming locomotion for autonomous underwater robots: a review and a novel solution to improve control and efficiency. Ocean Eng. **130**, 437–453 (2017)
7. Barrett, D.S.: The design of a flexible hull undersea vehicle propelled by an oscillating foil. Massachusetts Institute of Technology Department of Ocean Engineering (1994)
8. Hirata, K.: Development of experimental fish robot. In: Sixth International Symposium on Marine Engineering (ISME 2000), Tokio, pp. 23–27 (2000)

9. Anderson, J.M., Narender, K.C.: Maneuvering and stability performance of a robotic tuna. Integr. Comp. Biol. **42**(1), 118–126 (2002)
10. Fukuda, T. et al.: Mechanism and swimming experiment of micro mobile robot in water. In: IEEE Workshop on Micro Electro Mechanical Systems, MEMS'94, Proceedings. IEEE, pp. 273–278 (1994)
11. Suleman, A., Crawford, C.: Studies on hydrodynamic propulsion of a biomimetic tuna. In: Inzartsev, A.V. (ed.) Underwater Vehicles, pp. 459–486 (2008)
12. Kodati, P., Hinkle, J., Winn, A., Deng, X.: Microautonomous robotic ostraciiform (MARCO): hydrodynamics, design and fabrication. IEEE Trans. Robot. **24**(1), 105–117 (2008)
13. Epps, B.P., Valdivia y Alvarado, P., Youcef-Toumi, K., Techet, A.H.: Swimming performance of a biomimetic compliant fish-like robot. Experimental Fluids **47**(6), 927–939 (2009)
14. Stefanini, C., Orofino, S., Manfredi, L., Mintchev, S., Marrazza, S., Assaf, T., Capantini, L., Sinibaldi, E., Grillner, S., Wallén, P., Dario, P.: A novel autonomous, bioinspired swimming robot developed by neuroscientists and bioengineers. Bioinspir. Biomim. **7**(2) (2012)
15. Kruusmaa, M., Fiorini, P., Megill, W., De Vittorio, M., Akanyeti, O., Visentin, F., Chambers, L., El Daou, H., Fiazza, M.-C., Jezov, J., Listak, M., Rossi, L., Salumae, T., Toming, G., Venturelli, R., Jung, D., Brown, J., Rizzi, F., Qualtieri, A., Maud, J., Liszewski, A.: Filose for svenning: a flow sensing bioinspired robot. IEEE Robot. Autom. Mag. **21**(3), 51–62 (2014)
16. Lighthill, M.J.: Note on the swimming of slender fish. J. Fluid Mech. **9**(2), 305–317 (1960)
17. Lighthill, M.J.: Large-amplitude elongated-body theory of fish locomotion. Proc. R. Soc. Lond. B Biol. Sci. **179**(1055), 125–138 (1971)
18. Tzeranis, D., Papadopoulos, E., Triantafyllou, G.: On the design of an autonomous robot fish. In: Proceedings of the 11th IEEE Mediterranean Conference on Control and Automation (MED 2003), Rhodes, pp. 17–20 (2003)
19. Yu, J., Long, W.: Parameter optimization of simplified propulsive model for biomimetic robot fish. In: Proceedings of the 2005 IEEE International Conference on Robotics and Automation (ICRA 2005), Barcelona, pp. 3306–3311 (2005)
20. Liu, J., Huosheng, H.: Biological inspiration: from carangiform fish to multi-joint robotic fish. J. Bionic Eng. **7**(1), 35–48 (2010)
21. Blake, R.W.: On ostraciiform locomotion. J. Mar. Biol. Assoc. UK **57**(4), 1047–1055 (1977)
22. Costa, D., Palmieri, G., Palpacelli, M.-C., Callegari, M., Scaradozzi, D.: Design of a bio-inspired underwater vehicle. In: 12th IEEE/ASME International Conference on Mechatronic and Embedded Systems and Applications (MESA 2016), IEEE (2016)
23. Triantafyllou, M.S., Triantafyllou, G.S.: An efficient swimming machine. Sci. Am. **272**(3), 64–71 (1995)
24. Franklin, J.: Ingenious Mechanisms for Designers and Inventors. Industrial Press (1930)
25. Allotta, B., Caiti, A., Chisci, L., Costanzi, R., Di Corato, F., Fantacci, C., Fenucci, D., Meli, E., Ridolfi, A.: Development of a navigation algorithm for autonomous underwater vehicles. In: IFAC Workshop on Navigation, Guidance and Control of Underwater Vehicles (NGCUV 2015), Girona, vol. 28(2), pp. 64–69 (2015)
26. Allotta, B., Costanzi, R., Ridolfi, A., Reggiannini, M., Tampucci, M., Scaradozzi, D.: Archaeology Oriented Optical Acquisitions through MARTA AUV during ARROWS European Project Demonstration. In: MTS/IEEE OCEANS 2016, Monterey, pp. 1–4 (2016)
27. Conte, G., De Capua, G.P., Scaradozzi, D.: Designing the NGC system of a small ASV for tracking underwater targets. Robot. Auton. Syst. **76 I. C**, 46–57 (2016)
28. Conte, G., Gambella, L., Scaradozzi, D., Zanoli, S., Caiti, A., Calabrò, V., Alcocer, A., Alves, J., Cardeira, B., Cunha, R., Curado, F., Oliveira, P., Oliveira, A., Pascoal, A., Rufino, M., Sebastïo, L., Silvestre, C.: Underwater vehicle technology in the European research project VENUS. Underw. Technol. **28**(4), 175–185 (2009)
29. Conte, G., Scaradozzi, D., Sorbi, L., Panebianco, L., Mannocchi, D.: ROS Multi-agent structure for autonomous surface vehicles, MTS/IEEE OCEANS 2015 Genoa (2015)
30. Scaradozzi, D., Sorbi, L., Conte, G.: Assisted guidance system for micro ROV in underwater data gathering missions. In: Proceedings of the 20th Mediterranean Conference of Control and Automation (MED 2012), Barcelona, pp. 1373–1378 (2012)
31. Morganti, G., Perdon, A.M., Conte, G., Scaradozzi, D.: Multi-agent system theory for modelling a home automation system. In: Lecture Notes in Computer Science (Including Subseries Lecture Notes in Artificial Intelligence and Lecture Notes in Bioinformatics), 5517 LNCS (Part 1), pp. 585–593 (2009)
32. Wooldridge, M.: An introduction to muliagents systems. Wiley (2009)
33. Eloy, C.: Optimal strouhal number for swimming animals. J. Fluids Struct. **30**, 205–208 (2012)
34. Lamb, H.: Hydrodynamics. Cambridge University Press (1932)

Daniele Costa attained his master's degrees in Aerospace Engineering from Politecnico di Milano in 2011; in 2015 he attained his second master's degree in Mechanical Engineering from the Polytechnic University of Marche, Ancona, Italy. Since the month of November 2015, he has been attending the Ph.D. Course in Mechanical Engineering. His fields of research are mainly the analysis and design of bio-inspired propulsive mechanisms for underwater locomotion. He is also focused on the study of robotics, particularly on those operating in the marine environment.

Giacomo Palmieri received the Ph.D. degree in mechanical engineering from the Polytechnic University of Marche, Ancona, Italy, in 2010. He has been an Assistant Professor in Machine Mechanics at Polytechnic University of Marche since 2016. He participated in a national research program on micro-manipulation and assembly. His research interests include engineering aspects on machine mechanics and biomechanics. Main topics are dynamics of human motion, parallel kinematics machines, minirobotics, visual control of robots.

Matteo-Claudio Palpacelli is assistant professor in Machine Mechanics at the Department of Industrial Engineering and Mathematical Sciences of Polytechnic University of Marche in Ancona, Italy, since 2008. He received his Ph.D. in Artificial Intelligent Systems in 2008 from the same university. He participated to research programs on mini/micro robotics and process automation in textile industry funded by Italian and European communities. His main fields of research are the analysis and synthesis of parallel kinematics machine, the analysis and design of mechatronic systems and the dynamics of multibody mechanical systems.

Luca Panebianco is a Ph.D. student at the Polytechnic University of Marche, Ancona, Italy. He received his master's degrees in Automation and Information Engineering from the same faculty. His field of research regards the design and development of solutions to address cooperation, collaboration and modularity to a wide range of autonomous vehicles by means of the Multi-Agent System theory. Since October 2015, he has been collaborating to the development of the DocuScooter, a modular and low-cost platform dedicated to the data acquisition from the marine environment, as part of the GreenBubbles project.

David Scaradozzi, Ph.D., is Assistant Professor in Design and Optimization of Control Systems at Polytechnic University of Marche, Ancona, Italy. He was technical manager in VENUS FP7 European Project. He is principal investigator of UnivPM in the projects: Sunrise for study and development of underwater optical modems, GreenBubbles for study and development of innovative robotic tools for social science and Lab4Dive for development of a Mobile Smart Lab for Augmented Archaeological Dives. His research activities are in the field of control and optimization of dynamical systems; robotics and automation, with special interests devoted to all the aspects involving planning, motion and interaction control problems in distributed agents, rapid prototyping, mechatronics and home automation; educational robotics, with special interests devoted to all the aspects of new robotics tools development for teaching e-STrEM subjects.